ESR and OSL dating of fossil-bearing deposits from Naracoorte Cave Complex palaeontological sites, South Australia

Priya[1] *, Arnold, L.J.[1], Guilarte, V.[2], Duval, M.[3,4], Demuro, M[1], Weij, R.[5], Reed, E.H.[6,7]

[1]School of Physical Sciences, Environment Institute, and Institute for Photonics and Advanced Sensing (IPAS), University of Adelaide, Adelaide, South Australia, Australia.
[2] Facultad de Ciencias de la Educación y del Deporte de Melilla, Universidad de Granada, Spain
[3]Centro Nacional de Investigación sobre la Evolución Humana (CENIEH), Burgos, Spain.
[4]Australian Research Centre for Human Evolution (ARCHE), Griffith University, Brisbane, Australia.
[5]School of Geography, Earth and Atmospheric Sciences, University of Melbourne, Parkville, Victoria, Australia
[6]School of Biological Sciences, Environment Institute, University of Adelaide, Adelaide, Australia.
[7]South Australian Museum, Adelaide, South Australia, Australia.
*Corresponding Author: priya@adelaide.edu.au

Abstract

Little work has been undertaken on combined dating of sedimentary quartz grains using electron spin resonance (ESR) and optically stimulated luminescence (OSL) techniques in Australia. This study aims to assess the suitability of a combined ESR and OSL dating approach for establishing improved chronologies of Middle-Late Pleistocene deposits within the Naracoorte Cave Complex (NCC), South Australia. Here, we apply ESR and OSL dating in tandem to a series of samples collected from three different NCC sites: Whale Bone, Specimen and Alexandra cave. ESR quartz dating focuses on the multi-centre (MC) approach, which involves comparative evaluations of Al and Ti centre signals, while paired luminescence dating focuses on single-grain OSL analysis and includes examination of multi-grain averaging effects. The comparative ESR-OSL dating results exhibit broad agreement for deposits spanning 50-150 thousand years, with either the Ti-H or Al centre ages overlapping with paired OSL ages at 2σ in nearly all cases. MC ESR evaluations (Al v Ti-Li v Ti-H age assessments) indicate incomplete resetting of the bleachable Al centre signal for a small number of samples. Two-thirds of samples exhibit Ti-Li ages that are apparently older (although within 2σ error) than corresponding Al centre ages, which is unexpected from a bleaching kinetics perspective and may indicate a broader reliability issue for Ti-Li palaeodose evaluation with these particular samples. Our findings: (i) support the applicability of both palaeodosimetric dating methods in this depositional setting; (ii) highlight the merits of applying combined ESR-OSL analyses in tandem, and; (iii) provide one of the first reliable MAAD evaluations of quartz ESR MC dating for samples with natural dose ranges as low as only a few tens of Gy. These results show that the Whale Bone, Specimen and Alexandra cave sites are temporally related and can be used to derive multi-site reconstructions of faunal assemblages and palaeoenvironmental history.

Keywords: Quartz ESR dating; Multi-centre approach, single-grain OSL dating; Naracoorte cave

1. Introduction

Combined application of electron spin resonance (ESR) and optically stimulated luminescence (OSL) dating of quartz grains – the two most widely used quartz dating techniques in Quaternary studies – can provide improved insights into methodological reliability over Middle to Late Pleistocene timescales. Comparisons of optically bleached quartz dating methods using shared sedimentary samples offer optimal assessments of dating reliability by enabling stratigraphically constrained evaluations of dose rate or palaeodose complications that may otherwise be difficult to unravel in certain depositional settings (Demuro et al., 2020a). In spite of these advantages, stratigraphically paired evaluations of ESR and OSL dating remain relatively uncommon (Demuro et al., 2020b; Tanaka et al., 1997; Tissoux et al., 2010). In Australia, relatively little work has been undertaken on ESR dating of sedimentary quartz (Beerten et al., 2008; Rink et al., 2007; Tanaka et al., 1995; Yoshida, 1996) and there have been even fewer comparative studies of multiple centre (MC) ESR and OSL dating techniques (Beerten et al., 2006; Rittner, 2013).

The Naracoorte Cave Complex (NCC) of South Australia comprises >150 cave sites (White and Webb, 2015), many of which contain extensive infill sequences with rich megafauna fossil assemblages spanning the last 550 thousand years. This karst system is considered a key fossil locality for understanding the drivers of Australia-wide Late Pleistocene megafaunal extinction given the presence of numerous, overlapping fossil sites in direct association with well-stratified palaeoenvironmental proxies. An extensive radiometric dating program is currently in progress to improve chronological constraints on a large number of NCC cave sites (e.g. Arnold et al., this volume). Establishing reliable chronologies on the NCC fossil-bearing deposits using quartz trapped charge dating techniques is critical since most NCC sites lie close to, or well-beyond, the radiocarbon dating range (Grün et al., 2001; Moriarty et al., 2000; Prideaux et al., 2007).

In this study, we focus on three of these Middle-Late Pleistocene NCC sites that share similar types of deposits (sediment cones associated with solution pipe entrances) and potentially contemporaneous faunal assemblages currently lacking robust chronostratigraphic frameworks: Whale Bone, Specimen and Alexandra Caves. Palaeontological excavations are currently being undertake in Whale Bone and Specimen caves, hence establishing a firm dating framework is important for guiding ongoing research programs.

The main aim of the study is to assess the suitability of a combined ESR and OSL dating approach for establishing improved chronologies at NCC sites. This is achieved by applying complementary ESR MC and single-grain OSL techniques to splits of the same samples to minimise stratigraphic uncertainties. U/Th dating of a closely associated speleothem is also undertaken at Specimen Cave to provide independent age control. These comparative dating assessments are used to: (1) evaluate characteristics of radiation-induced ESR signals associated with quartz $[AlO_4]^0$ and $[TiO_4/M^+]^0$ (M^+= Li^+ and H^+) paramagnetic centres (simplified as Al and Ti centres below); (2) examine ESR signal bleaching adequacy, dose response properties and dating reliability over relatively low natural dose ranges; (3) provide insights into potential multi-grain OSL averaging effects for NCC deposits; (4) Establish improved chronological constraints for sedimentary and fossil deposition in the three cave sites, thereby expanding the existing NCC chronostratigraphic framework.

2. Study context and sample details

The three NCC fossil deposits at Alexandra, Specimen and Whale Bone Caves have all accumulated via narrow solution pipe entrances that acted as pitfall traps for vertebrates and sources for sediment cone deposition. Alexandra Cave has an exposed sedimentary section that is laterally continuous for 30 m in the entrance chamber (McCluskey, 2012). Previous study of the cave deposit attributed the sediment source to be alluvial and colluvial, with chronology from radiocarbon ages on charcoal constraining the top 1.9 m of the sediment sequence to 17.5 – 30.8 thousand years ago (ka) (Table S6; McCluskey, 2012). Vertebrate fossils recovered during excavations indicate a diverse mammal fauna including megafaunal species *Thylacoleo carnifex* (an extinct marsupial carnivore), and two extinct short-faced kangaroos, *Procoptodon goliah* and *Simosthenurus occidentalis* (Reed and Bourne, 2000). The presence of extinct megafauna taxa provides a *terminus ante quem* age estimate of 36.7 – 48.1 ka (Saltré et al., 2016) for the part of the sequence located beneath a depth of 1.9 m (Table S6). Four sediment samples were collected from Alexandra Cave to provide sufficient coverage of the stratigraphic sequence (Fig. 1) located below the first 1.9 m previously dated by radiocarbon. The lowermost sample (ALEX19-10) was collected from the base of the exposed sequence to constraint the initial phase of sedimentary infilling. Samples ALEX19-3 and ALEX19-6 were collected to bracket the lower and intermediate palaeontological levels.

Specimen Cave consists of a solution pipe leading to a large chamber containing a >1 m thick clastic fossil deposit in the southwest corner, which is capped by an extensive (30-40 cm-thick) flowstone layer. A small excavation was undertaken in the cave in 1908 and yielded megafauna fossils from *Thylacoleo carnifex, Protemnodon sp.* and *Simosthenurus* sp. (Reed and Bourne, 2000). New excavations are currently underway in the cave. A single ESR-OSL dating sample (SPEC18-2) was collected from the uppermost layer of the current site excavation to provide terminal age constraint for the fossil deposit. In addition, two U-Th samples (SP-18 and SP-17) were extracted from the top- and mid-section of the closely related speleothem formation. Sample SPEC18-2 was taken 55 cm beneath the base of this speleothem and ~1.5 m to the side of the U-Th sampling positions. Further details of the U-Th methods and results obtained for these two samples are provided in S.M.5.

Whale Bone Cave contains a smaller sediment cone deposit that is currently classified as a single stratigraphic unit. The ~1 m-thick fossil sequence contains abundant extinct Pleistocene vertebrate remains, including *Phascolarctos cinereus, Thylacoleo carnifex, Macropus fuliginosus, 'Procoptodon' browneorum* and '*Procoptodon' gilli* (Reed and Bourne, 2009). There is currently no available numerical age control for the fossil deposit, though the presence of extinct megafauna indicates an expected age of >36.7 ka (Saltré et al., 2016). A single ESR-OSL dating sample (WBC19-1) was collected from the uppermost exposed layers of the main excavation (10 cm beneath the surface) to constrain the last appearance of megafauna at the site.

3. Experimental procedures

Samples were prepared under safe-light conditions according to standard laboratory procedures outlined in Aitken (1985) (see Fig. S2 for details), and the resulting purified quartz grains of each sample were split for luminescence and ESR analyses.

ESR dose evaluation was performed on varying grain size fractions of quartz (Table 1) at the Australian Research Centre for Human Evolution, Griffith University, using the standard multi-grain multiple aliquot additive dose (MAAD) method. ESR measurements were performed using an Elexsys E 500 Bruker X-band ESR spectrometer at low temperature (77 K) using a finger dewar filled with liquid nitrogen (see details of the experimental setup and performance in Guilarte et al., submitted). In accordance with the MC approach (Toyoda et al., 2000), the radiation-induced ESR signals associated with the Al, Ti (option D) and Ti-H centres were acquired in a single spectrum and measured as per Bartz et al. (2020) (see an example in Fig. S3). The full analytical procedure is provided in the Supplementary Information (*S.M.2. ESR dating*).

Single-grain (SG) OSL analyses were undertaken on the 212 – 250 µm quartz fraction (90 – 250 µm quartz fraction for WBC19-1) in the Prescott Environmental Luminescence Laboratory at the University of Adelaide. Equivalent dose (D_e) measurements were conducted on 500 – 1500 grains/sample for SG OSL analysis, while multi-grain (MG) OSL analysis of the Alexandra Cave samples was undertaken using a 5 mm mask size (approximately 500 grains/aliquot). D_e values were determined using the SAR protocol shown in Table S2 and the analytical procedures of Arnold et al., 2016, 2012a), which are further detailed in the Supplementary information (*S.M.3. OSL dating*).

Environmental dose rate assessments were conducted in tandem for the ESR and OSL sample splits. As such, the only differences between the ESR and OSL dose rates for a given sample relate to grain-size attenuation effects and alpha efficiency values. Field gamma dose rate measurements were made using a portable gamma spectrometer NaI:Tl detector connected to an InSpector 1000 digital handheld multichannel analyser. The 'energy windows' approach described in Arnold et al. (2012b) and Duval and Arnold (2012) was used to derive individual estimates of U, Th and K concentrations from the field gamma-ray spectra. External beta dose rates were calculated from measurements made on a Risø GM-25-5 beta counter, using homogenised sediment sub-samples collected from the main ESR-OSL dating sample positions. Radionuclide concentrations have been converted to dose rates using the conversion factors given in Guérin et al. (2011), making allowance for beta-dose attenuation (Mejdahl, 1979; Brennan, 2003). Cosmic-ray dose rates were calculated using the approach described in Prescott and Hutton (1994), taking into consideration the site altitude, geomagnetic latitude as well as the density, thickness and geometry of sediment and bedrock above the sample. The gamma, beta and cosmic-ray dose rates are corrected for long-term sediment water content (Aitken, 1985). Further details of dose rate evaluations are given in Table 1.

4. Results

3.1. *ESR dating*

3.1.1. ESR dose determination

All ESR dose response curves obtained for the Al, Ti (D) and Ti-H signals are displayed in Fig. S4 to S9, while numerical fitting results are given in Table S1. Bleaching coefficient values obtained from the Al signal (expressed as the relative difference between the ESR intensities of the natural and the bleached aliquots), range from 39 % to 70 %, suggesting highly variable bleaching conditions for all samples, while no apparent stratigraphic trend is observed for the samples from Alexandra Cave. Measurement repeatability for the Al signal ranges from 1.1% to 11 %, resulting in D_e variability of between 11% and 14 %, which is within the standards usually obtained for this centre. The exception is WBC 19-1, which shows significantly enhanced D_e precision (5 %). The Ti centre (option D) has a measurement repeatability of 1–6 %, and D_e repeatability of 3–13 % (Table S1), which is slightly better than the Al centre. In particular, four out of six samples show excellent D_e repeatability (<10%). The Ti-H centre has a measurement repeatability of 1–6 %, and D_e repeatability of 6–25 % (Table S1). In comparison to the Al and Ti (D) centres, the average intensity repeatability of the Ti-H centre is superior (2.6%), though its D_e repeatability is inferior (14.7 %) as a result of weaker signal intensity and higher signal-to-noise ratio (see example in Fig. S3).

The Al centre D_e values were obtained by fitting an exponential + linear (EXP+LIN) fitting function (data weighted by inverse of the squared intensities, $1/I^2$) through the pooled repeated ESR intensities, with a maximum applied irradiation dose (D_{max}) of 12000 Gy. The calculated D_e values are in the range of 27 ± 1.9 – 141 ± 13.4 Gy (Table S1). Only SPEC 18-2 had an adjusted r^2 value <0.98, suggesting overall reliable fitting results for the combined dataset.

The Ti (D) and Ti-H signal D_e values were obtained using both Ti-2 and single saturating exponential (SSE) functions as described in Duval and Guilarte (2015). The Ti (D) ESR intensities do not exhibit the decreasing dose-dependency behaviour typically observed at high dose values (Fig. S6, S7); therefore, the Ti-2 fitting function cannot be employed for these samples. Similar atypical behaviour has been observed in previous studies (e.g., Duval et al., 2017) and is likely a result of the limited D_{max} value employed here (12000 Gy). The SSE fitting function is more appropriate to describe the experimental data points showing apparent dose saturation. Since this function can potentially return overestimated D_e values when adopting inappropriate D_{max} values (e.g., Duval et al., 2009), the evolution of both parameters (D_e and D_{max}) for Ti (D) is plotted in Fig. S10. The impact of D_{max} was assessed by performing the SSE fitting repeatedly after removing successive data points from the high dose range. Interestingly, all samples show a similar trend, with D_e values remaining relatively constant (or within error) up to D_{max} = 1000-3000 Gy, followed by a significant increase at higher doses. The strong correlation between D_e and D_{max} values shows that the SSE function is not appropriate to describe the behaviour of the ESR intensities for D_{max} > 3000 Gy. In contrast, the resulting D_e value reaches a plateau in the < 1000-3000 Gy dose range (note the large D_e errors for D_{max} < 1000 Gy as a result of the limited number of data points available for the fitting), indicating the absence of significant correlation between D_e and D_{max}. Consequently, a D_{max} value of 1522 Gy was used for most samples, as this produced the lowest inter-sample variability, while D_{max} values of 2978 Gy and 997 Gy were used for Alex 19-8 and WBC 19-1, respectively.

Since the Ti-H signal typically reaches apparent saturation much earlier than the Ti (D) signal (usually in the 3000-6000 Gy dose range; see Duval and Guilarte, 2015), slight decreasing dose-dependency behaviour is observed in the DRCs (Figs. S8, S9) for this signal. Consequently, the standard Ti-2 fitting function can be used for the Ti-H data obtained here (Duval and Guilarte, 2015); although the fitting of the decreasing dose component can only be achieved with a very limited number of points (1 or 2), which may result in significant uncertainty in the fitting results. As such, all Ti-H DRCs were fitted with both SSE (with increasing D_{max} from 403 to 11995 Gy) and Ti-2 functions (over the full dose range, with D_{max} =11995 Gy) for comparison (Fig. 2). Excluding the scattered D_e values derived using D_{max} = 403 and 606 Gy, which is the result of having very few experimental data points, produces relatively constant D_e values for all samples in spite of the increase in D_{max} from 998 to 11995 Gy (which is unlike the Ti (D) signal). The D_{max} value therefore has limited influence on D_e values for the SSE fitting results, suggesting that the use of this function is appropriate to describe the data set. These Ti-H D_e values are in the range of 26.1 ± 1.3 – 128.1 ± 9.5 Gy and 25.3 ± 1.3 – 138.1 ± 7.7 Gy for the SSE and Ti-2 functions, respectively (Table S1). Interestingly, both the SSE (D_{max} =1522 Gy) and Ti-2 functions yield consistent D_e values at 1σ for three out of six samples, while all replicate results are in agreement at 2σ. The magnitude of the D_e estimates for these samples are all within the range of values (<300-400 Gy) for which the Ti-H signal is known to provide reliable dose estimates (Bartz et al., 2020).

3.1.2. Multiple centre approach

The Ti-H centre signal consistently produces the lowest D_e values of the ESR MC dataset, while the Ti (D) signal provides, somewhat unexpectedly, the highest D_e values; although similar trends have been observed in other studies (e.g. Asagoe et al., 2011; Beerten et al., 2006; Beerten and Stesmans, 2007; Rittner, 2013; Tissoux et al., 2007, 2008). Importantly, however, the D_e derived from the Ti (D) and Al signals are consistent at 2σ for all six samples (Fig. S11), which suggests that these systematic differences may not be significant. This observed D_e pattern is consistent with the known respective bleaching rates of each signal, with the Ti-H signal achieving full resetting much faster than any other signal (Rink et al., 2007; Tissoux et al., 2007). It is also worth noting that other sources of uncertainty might have partially impacted the MC fitting results in this study. In particular, the low natural dose ranges under consideration here (<150 Gy) are especially challenging from an ESR methodological perspective. This could result in curve fitting artefacts and an inability to accurately determine D_e values for the Al and Ti (D) centres, given the existing uncertainty on the ESR intensities (typically, a few %) and the lower radiation sensitivity of these two signals compared with that of Ti-H (Duval and Guilarte, 2015).

3.2. *OSL dating*

The SG-OSL D_e distributions show that five of the six samples (ALEX19-3, ALEX19-8, ALEX19-10, SPEC 18-2, WBC 19-1) are well bleached and have not been affected by syn-depositional mixing complications (Fig. S13). The overdispersion values for these samples range between 26 ± 2 and 33 ± 2% (Table 1), and are in agreement with values commonly reported for ideal (well-bleached and unmixed) sediment samples (e.g. Arnold et al., 2019), including those from other NCC sites (Arnold et al., this volume). Sample ALEX19-6 is an exception to this trend, exhibiting a notably higher overdispersion of 41 ± 2% (Table 1), a significant positively skewed D_e distribution according to the test of Bailey and Arnold (2006) and Arnold et al. (2011), and a maximum log likelihood (L_{max}) test score (Arnold et al., 2009) favouring use of the minimum age model (MAM; Galbraith et al., 1999) over the weighted mean (central age model; CAM) for D_e evaluation. These characteristics suggest that ALEX19-6 may have been affected by more significant syn-depositional mixing (i.e., mixing of pre-existing cave sediments with externally derived quartz grains during their initial transportation within the cavity; e.g. (Arnold et al., 2019) or bleaching complications compared to other samples. This interpretation is supported by the scattered replicate D_e distributions obtained for this sample using single-grain thermally transferred OSL (TT-OSL) and post-infrared infrared stimulated luminescence (pIR-IRSL) (Arnold et al., this volume). It is also consistent with the sedimentological characteristics of the ALEX 19-6 host deposits, which (unlike the other sampled deposits) lack bedding structures (laminations, charcoal bands) and likely indicate a higher-energy depositional environment that could have contributed to syn-depositional mixing.

The replicate MG-OSL ages obtained for four of the Alexandra Cave samples provide useful insights into multi-grain averaging effects for NCC deposits. The MG-OSL ages for ALEX 19-3 and ALEX 19-6 are in agreement with their SG-OSL counterparts, confirming the suitability of both approaches for D_e determination. However, the MG-OSL ages for ALEX 19-8 and ALEX 19-10 are significantly (~50%) higher than the corresponding SG-OSL ages. The reason for this upward shift in MG-OSL ages can be gleaned by examining the characteristics of the rejected grains populations (Table S4). In particular, a significantly higher proportion of measured grains for samples ALEX 19-8 and ALEX 19-10 are rejected for exhibiting aberrant luminescence properties associated with high sensitivity-corrected natural signals; namely, non-intersecting, extrapolated and saturated grains (e.g. Fig. S12). The number of rejected grains falling into this category amounts to ~50-62% of the accepted grain populations for samples ALEX19-8 and ALEX19-10, compared to only 1-3% of the accepted grain populations for samples ALEX 19-3 and ALEX 19-6 (Table S4). While these unreliable grains can be routinely rejected during SG-OSL analysis, they cannot be excluded from MG OSL measurements and thus contribute to a significant upward shift in the cumulative sensitivity-corrected natural signals of the final MG-OSL D_e datasets for ALEX 19-3 and ALEX 19-6. The same type of biasing MG averaging effects have been reported elsewhere for samples that contain significant populations of non-intersecting, extrapolated and saturated grain types (Arnold et al., 2012a, 2013).

Discussion

4.1. *ESR-OSL comparisons*

There is good overall agreement between the ESR (Ti-H) and SG OSL ages at the three study sites (Table 1; Fig. 3). For SPEC 18-2, the ESR (Ti-H) and OSL results are additionally compatible with U-series ages from a calcite flowstone directly above the sample (Table 1), whereas both the Al and Ti (D) ESR ages overestimate the independent age control. This confirms that these two ESR signals have most likely not been fully reset during sediment transport.

The SG OSL analysis similarly show that the sampled sediments are generally well-bleached and unlikely to have been affected by syn-depositional mixing, with the exception of ALEX 19-6 (Table 1; Fig S13). Given the depositional context and related sedimentological evidence, the D_e scatter observed for ALEX 19-6 is likely the result of mixing with previously deposited sediments during transportation through the cave or partial bleaching of sediments prior to deposition. Interestingly, the corresponding ESR MC ages for sample ALEX19-6 do not appear to exhibit any overestimation compared to the SG-OSL age, which might otherwise be expected if they have experienced the same depositional history (especially given MG averaging effects). It is possible that the coarser grain fraction used for the SG-OSL analysis (212 – 250 µm) is more susceptible to progressive, short-distance mobilisation through the cave system during successive high-energy transportation events compared to the finer grain fraction used for the ESR analysis (125 – 212 µm). The latter would certainly have lower entrainment thresholds and thus may be transported more directly through the cave system during single flow events. Such sediment routing grain-size dependencies remain largely unexplored in karst settings, but should be investigated further using replicate OSL or ESR measurements performed on various grain size fractions.

The results of the SG-OSL versus MG-OSL comparisons reveal that some NCC deposits may suffer from adverse multi-grain averaging effects that could affect the reliability of conventional OSL dating in this setting. Complex MG-OSL averaging effects related to the inclusion of aberrant grain types have been widely reported (Arnold et al., 2012a, 2013, 2016, 2019; Demuro et al., 2013, 2008; Jacobs et al., 2006; Russell and Armitage, 2012; Stone and Bailey, 2012). Our results indicate the potential for systematic biases associated with large populations of non-intersecting, extrapolated and saturated grain types, and suggest it may be prudent to focus on SG-OSL rather than MG-OSL analysis for NCC deposits. It is plausible that the same upward shift in MG-OSL ages observed for samples ALEX19-8 and ALEX19-10 may explain the 10 – 25 ka overestimation of MG-OSL ages reported previously at the nearby NCC site of Blanche Cave (Darrénougué et al., 2009). Unfortunately, it remains unclear whether multi-grain ESR signals are similarly affected by adverse averaging effects related to unsuitable grain types. This is conceivable (e.g., Beerten and Stesmans, 2006a, 2006b), and could contribute to some of the systematic differences observed with ESR MC ages (assuming such averaging effects affect the Ti-H, Ti (D) and Al ESR signals to differing extents). However, this would need to be specifically investigated using ESR single-grain analysis before drawing any further conclusions.

A potential explanation for the systematically older Ti (D) ages observed in this study (Fig. 3), is that this particular ESR signal is not fully bleached, and retains a residual (unbleached) dose prior to burial (Tissoux et al., 2007; Toyoda et al., 2000). Beerten et al. (2006) showed Ti-Li residual signals of up to 70% of the natural (option E from Duval & Guilarte 2015). Richter and Tsukamoto (2021) showed residual doses in all centres (86 – 2039 Gy), including for the Ti-H signal (86 – 263 Gy). Measurements of residual dose in modern analogue samples have also showed residual doses of 61 – 466 Gy for the Ti-Li signal (option D from Duval & Guilarte 2015) (Tsukamoto et al., 2017). However, if the Ti (D) ESR signal had not been fully reset prior to sediment deposition, it is expected that incomplete bleaching would also apply to the Al signal, which has much slower bleaching kinetics, and would have a larger D_e value than the Ti (D) signal, contrary to the results observed in this study. While incomplete bleaching of the Ti (D) signal is unlikely, a study on modern analogue sediment samples from NCC would enable improved evaluations of the ESR Ti (D) signal.

Another possible explanation for the systematically older Ti (D) ages observed in this study could relate to the relatively large intensity of Ti-H and Ti-Li signals, which may impact the accuracy of the dose estimates derived from each centre. Beerten and Stesmans (2006b) observed that for samples with both Ti-H and Ti-Li signals, the latter provided overestimated dose estimates, while no significant bias was observed in samples that did not have a Ti-H signal. The Naracoorte samples are characterised by exceptionally high Ti-H intensities, despite their relatively young ages, which may impact Ti-Li centre signal evaluation. In particular, the C/D intensity ratio (Duval and Guilarte, 2015) calculated for the NCC natural samples are exceptionally high (0.9 to 1.22) compared to those observed in quartz from other localities (Duval and Guilarte, 2015; Demuro et al., 2020b). This variability in C/D intensity ratio likely relates to the nature and origin of the quartz being dated (see comparative data in Bartz et al., 2020; Demuro et al., 2020b), and suggests that the NCC samples considered in this study might be more susceptible to the complications suggested by Beerten and Stesman (2006a).

The measurement of Ti ESR intensities can vary between studies (see Duval et al., 2020), making comparisons across sites difficult. Depending on how the ESR intensities are measured (see options A – E Duval and Guilarte, 2015) and the source of quartz (Demuro et al., 2020b), the relative contribution of Ti-H and Ti-Li signals may vary. Standardising the evaluation of ESR intensities within the dating community could help to improve our understanding of the nature and composition of ESR signals related to Ti centres.

Taking these various factors into consideration, it seems likely that the Ti (D) D_e overestimations observed for the NCC samples relate to their high Ti-H signal intensities and related adverse impacts on Ti (D) ESR evaluation, rather than incomplete signal resetting during transport. Irrespective of the cause of the Ti (D) offset, the Al and Ti (D) signals ultimately produce age estimates that are within 2σ of each other. Hence, any apparent systematic differences observed with these samples are not statistically significant.

The Ti-H centre ages presented in this study are, to our knowledge, the youngest obtained so far using ESR dating with the MAAD method, providing reliable D_e estimates over natural dose ranges as low as < 30 Gy. These results confirm that the quartz preserved at NCC sites is particularly well suited for ESR dating, and that the Ti-H centre has great potential for dating Late Pleistocene NCC fossil deposits with corresponding burial doses < 100 Gy.

4.2. *Implications for NCC site histories*

The OSL and ESR ages provided in this study have extended the chronology of the Alexandra Cave entrance chamber sediment sequence by 130 ka; building on the initial radiocarbon ages of 17.5 – 30.8 ka (Table S6; McCluskey, 2012), we have established a basal age of 157.8 ± 9.8 ka (ALEX 19-10) for the lowermost sample in the stratigraphic section. This indicates that 6 m of sediment infill occurred at the site between marine isotope stage (MIS) 6 and MIS 2 (Lisiecki and Raymo, 2005), and confirms that the Alexandra Cave sequence spans multiple glacial-interglacial cycles. These chronological results are significant because they reveal that the deposit overlaps with the megafauna extinction period (36.7 – 48.1 ka) and >100 ka leading up to the event, flagging this sedimentary section as one of the few sites in Australia to enable detailed assessment of megafauna extinction dynamics over long timescales.

The Specimen Cave deposit was deposited during late MIS 6 or early MIS 5 (134.7 ± 8.7 ka), and can be chronologically correlated to the base of the Alexandra Cave entrance chamber deposit (Alex 19-10). Examining palaeoenvironment proxies from the infill sequence at Specimen Cave and Alexandra Cave would be useful to reconstruct regional climatic conditions during the MIS 6 to MIS 5 transition, as this time period is currently not represented by any other well-dated sedimentary deposits at NCC sites.

The Whale Bone Cave deposit is most likely constrained to the final stage of the last interglacial complex or the start of MIS 4, with mean ages centred on MIS 5a to 5b (71 – 87 ka). These ages overlap with the Alexandra Cave entrance chamber deposit presented here, and also Grant Hall chamber in Victoria Fossil Cave (Macken et al., 2011). Previous palaeoenvironmental and faunal studies at Grant Hall chamber suggested well-forested, dense woodlands (Fraser and Wells, 2006; Macken et al., 2011), with increased effective moisture during this period supported by speleothem deposition (Ayliffe et al., 1998). The extent of moisture availability during the last interglacial complex can be further assessed from the two newly identified MIS 5 cave sites presented in this study, Whale Bone and Alexandra caves, which share similar aged deposits.

The ages produced in this study contribute to the collective understanding of spatial and temporal relationships of NCC fossil sites (eg. Darrénougué et al., 2009; Forbes et al., 2007; Grün et al., 2001; Macken et al., 2011; St Pierre et al., 2012), opening up new possibilities for undertaking multi-site comparisons of faunal assemblages and palaeoenvironmental reconstructions spanning MIS 6 to 2, and improved scope for understanding the drivers of Australia-wide late Pleistocene megafauna extinction.

4. Conclusion

Comparative quartz ESR MC and OSL ages obtained on six NCC samples are in good agreement, with Ti-H and SG-OSL ages providing the closest age correspondence for the three study sites. This represents the first study to demonstrate the potential for obtaining reliable quartz Ti-H centre ages with the MAAD method over natural dose ranges as low as < 30 Gy. These promising results most likely reflect a combination of the experimental setup employed for cryogenic ESR measurements (finger dewar), which enabled data acquisition at much lower temperatures (77 K) and thus ensured higher signal intensity/resolution than with standard variable temperature units (see comparison study in Guilarte et al., submitted), and the favourable intrinsic ESR characteristics of the NCC quartz, which were found to be particularly well suited for ESR analyses.

SG and MG OSL comparisons show the advantages that SG OSL dating can offer for characterising and circumventing potentially biasing averaging effects for some NCC deposits. Further investigation into the potential for Ti (D) bleaching residuals and ESR multi-grain averaging effects would be worthwhile to expand the applicability of different MC signals at NCC sites.

The new SG-OSL and Ti-H chronologies presented here for Alexandra, Specimen and Whale Bone Cave constrain three previously undated megafauna fossil deposits to 50 – 150 ka, collectively spanning an important temporal gap in the existing NCC chronology. These results demonstrate the advantages of applying multiple palaeodosimetric dating techniques in tandem to examine methodological reliability and reconstruct more comprehensive sedimentary histories for late Pleistocene NCC deposits.

Acknowledgements

Financial support for this research was provided by Australian research Council (ARC) Linkage Project LP160101249 in conjunction with the Government of South Australia Department of Environment and Water, Naracoorte Lucindale Council, Terre a Terre Pty Ltd, Wrattonbully Wine Industries Association Inc, South Australian Museum, and Defence Science and Technology Group. We thank Tom Shortt, Peter Majoros, Nick McIntyre for facilitating research conducted at NCC sites. We are also grateful to Steve Bourne, Gilian Ross and Racheal Mahlknecht for their assistance with collecting, preparing and/or measuring the luminescence dating samples. MD's research is currently funded by the Spanish Ramón y Cajal Fellowship RYC2018-025221-I. The authors are grateful to María Jesús Alonso Escarza, CENIEH, for the UV bleaching experiment at CENIEH.

References

Aitken, M.J., 1985. Thermoluminescence dating / M.J. Aitken, Studies in archaeological science. Academic Press, London ; Orlando.

Arnold, L., Demuro, M., Power, R., Priya, Duval, M., Guilarte, V., Weij, R., Woodhead, J., White, L., Bourne, S., Reed, L., 2021. Examining sediment infill dynamics at Naracoorte Cave megafauna sites using multiple luminescence dating signals. Quat. Geochronol. This volume

Arnold, L.J., Demuro, M., Benito-Calvo, A., Pérez-González, A., Navazo, M., 2013. OSL dating of the Middle Palaeolithic Hotel California site, Sierra de Atapuerca, north-central Spain. Boreas.

Arnold, L.J., Demuro, M., Ruiz, M.N., 2012a. Empirical insights into multi-grain averaging effects from ‘pseudo’ single-grain OSL measurements. Radiat. Meas. 47, 652–658.

Arnold, L.J., Demuro, M., Spooner, N.A., Prideaux, G.J., McDowell, M.C., Camens, A.B., Reed, E.H., Parés, J.M., Arsuaga, J.L., Bermúdez de Castro, J.M., Carbonell, E., 2019. Single-grain TT-OSL bleaching characteristics: Insights from modern analogues and OSL dating comparisons. Quat. Geochronol. 49, 45–51. https://doi.org/10.1016/j.quageo.2018.01.004

Arnold, L.J., Duval, M., Demuro, M., Spooner, N.A., Santonja, M., Pérez-González, A., 2016. OSL dating of individual quartz ‘supergrains’ from the Ancient Middle Palaeolithic site of Cuesta de la Bajada, Spain. Quat. Geochronol. 36, 78–101.

Arnold, L.J., Duval, M., Falguères, C., Bahain, J.-J., Demuro, M., 2012b. Portable gamma spectrometry with cerium-doped lanthanum bromide scintillators: Suitability assessments for luminescence and electron spin resonance dating applications. Radiat. Meas. 47, 6–18. https://doi.org/https://doi.org/10.1016/j.radmeas.2011.09.001

Arnold, L.J., Roberts, R.G., Galbraith, R.F., DeLong, S.B., 2009. A revised burial dose estimation procedure for optical dating of youngand modern-age sediments. Quat. Geochronol. 4, 306–325. https://doi.org/https://doi.org/10.1016/j.quageo.2009.02.017

Arnold, L.J., Roberts, R.G., Maphee, R.D.E., Haile, J.S., Brock, F., Moller, P., Froese, D.G., Tikhonov, A.N., Chivas, A.R., Gilbert, M.T.P., Willerslev, E., 2011. Paper II – Dirt, dates and DNA: OSL and radiocarbon chronologies of perennially frozen sediments in Siberia, and their implications for sedimentary ancient DNA studies. Boreas 40, 417–445. https://doi.org/doi:10.1111/j.1502-3885.2010.00181.x

Asagoe, M., Toyoda, S., Voinchet, P., Falguères, C., Tissoux, H., Suzuki, T., Banerjee, D., 2011. ESR dating of tephra with dose recovery test for impurity centers in quartz. Quat. Int. 246, 118–123.

Ayliffe, L.K., Marianelli, P.C., Moriarty, K.C., Wells, R.T., McCulloch, M.T., Mortimer, G.E., Hellstrom, J.C., 1998. 500 ka precipitation record from southeastern Australia: Evidence for interglacial relative aridity. Geology 26, 147–150. https://doi.org/10.1130/0091-7613(1998)026<0147:KPRFSA>2.3.CO;2

Bailey, R.M., Arnold, L.J., 2006. Statistical modelling of single grain quartz De distributions and an assessment of procedures for estimating burial dose. Quat. Sci. Rev. 25, 2475–2502. https://doi.org/https://doi.org/10.1016/j.quascirev.2005.09.012

Bartz, M., Arnold, L., Spooner, N., Demuro, M., Campaña Lozano, I., Rixhon, G., Brückner, H., Duval, M., 2020. Publisher Correction: First experimental evaluation of the alpha efficiency in coarse-grained quartz for ESR dating purposes: implications for dose rate evaluation. Sci. Rep. 10, 5252. https://doi.org/10.1038/s41598-020-62007-w

Beerten, K., Lomax, J., Clémer, K., Stesmans, A., Radtke, U., 2006. On the use of Ti centres for estimating burial ages of Pleistocene sedimentary quartz: Multiple-grain data from Australia. Quat. Geochronol. 1, 151,158.

Beerten, K., Rittner, S., Lomax, J., Radtke, U., 2008. Dose recovery tests using Ti-related ESR signals in quartz: First results. Quat. Geochronol. 3, 143–149.

Beerten, K., Stesmans, A., 2007. ESR dating of sedimentary quartz: Possibilities and limitations of the single-grain approach. Quat. Geochronol. 2, 373–380.

Beerten, K., Stesmans, A., 2006a. Some properties of Ti-related paramagnetic centres relevant for electron spin resonance dating of single sedimentary quartz grains. Appl. Radiat. Isot. 64, 594–602. https://doi.org/10.1016/j.apradiso.2005.12.001

Beerten, K., Stesmans, A., 2006b. The use of Ti centers for estimating burial doses of single quartz grains: A case study from an aeolian deposit ~ 2 Ma old. Radiat. Meas. 41, 418–424.

Bowler, J.M., Johnston, H., Olley, J.M., Prescott, J.R., Roberts, R.G., Shawcross, W., Spooner, N.A., 2003. New ages for human occupation and climatic change at Lake Mungo, Australia. Nature 421, 837–840. https://doi.org/10.1038/nature01383

Brennan, B.J., 2003. Beta doses to spherical grains. Radiat. Meas. 37, 299–303. https://doi.org/10.1016/S1350-4487(03)00011-8

Darrénougué, N., De Deckker, P., Fitzsimmons, K.E., Norman, M.D., Reed, L., van der Kaars, S., Fallon, S., 2009. A late Pleistocene record of aeolian sedimentation in Blanche Cave, Naracoorte, South Australia. Quat. Sci. Rev. 28, 2600–2615. https://doi.org/https://doi.org/10.1016/j.quascirev.2009.05.021

Demuro, M., Arnold, L.J., Duval, M., Méndez-Quintas, E., Santonja, M., Pérez-González, A., 2020a. Refining the chronology of Acheulean deposits at Porto Maior in the River Miño basin (Galicia, Spain) using a comparative luminescence and ESR dating approach. Quat. Int. 556, 96–112.

Demuro, M., Arnold, L.J., Froese, D.G., Roberts, R.G., 2013. OSL dating of loess deposits bracketing Sheep Creek tephra beds, northwest Canada: Dim and problematic single-grain OSL characteristics and their effect on multi-grain age estimates. Quat. Geochronol. 15, 67–87. https://doi.org/https://doi.org/10.1016/j.quageo.2012.11.003

Demuro, M., Duval, M., Arnold, L.J., Spooner, N.A., Creighton, D.F., Méndez-Quintas, E., Santonja, M., Pérez-González, A., 2020b. Insights into the relationship between luminescence and ESR dating signals from Spanish sedimentary quartz samples of different geologic origins. Quat. Int. 556, 165–179.

Demuro, M., Roberts, R.G., Froese, D.G., Arnold, L.J., Brock, F., Ramsey, C.B., 2008. Optically stimulated luminescence dating of single and multiple grains of quartz from perennially frozen loess in western Yukon Territory, Canada: Comparison with radiocarbon chronologies for the late Pleistocene Dawson tephra. Quat. Geochronol. 3, 346–364.

Duval, M., Arnold, L., Rixhon, G., 2020. Electron spin resonance (ESR) dating in Quaternary studies: evolution, recent advances and applications. Quat. Int. 556. https://doi.org/10.1016/j.quaint.2020.07.044

Duval, M., Arnold, L.J., 2012. Field gamma dose-rate assessment in natural sedimentary contexts using LaBr3(Ce) and NaI(Tl) probes: A comparison between the “threshold” and “windows” techniques. Appl. Radiat. Isot. 74.

Duval, M., Arnold, L.J., Guilarte, V., Demuro, M., Santonja, M., Pérez-González, A., 2017. Electron spin resonance dating of optically bleached quartz grains from the Middle Palaeolithic site of

Cuesta de la Bajada (Spain) using the multiple centres approach. Quat. Geochronol. 37, 82–96. https://doi.org/https://doi.org/10.1016/j.quageo.2016.09.006

Duval, M., Grün, R., Falguères, C., Bahain, J.-J., Dolo, J.-M., 2009. ESR dating of Lower Pleistocene fossil teeth: Limits of the single saturating exponential (SSE) function for the equivalent dose determination. Radiat. Meas. 44, 477–482.

Duval, M., Guilarte, V., 2015. ESR dosimetry of optically bleached quartz grains extracted from Plio-Quaternary sediment: Evaluating some key aspects of the ESR signals associated to the Ti-centers. Radiat. Meas. 78, 28–41.

Forbes, M.S., Bestland, E.A., Wells, R.T., Krull, E.S., 2007. Palaeoenvironmental reconstruction of the Late Pleistocene to Early Holocene Robertson Cave sedimentary deposit, Naracoorte, South Australia. Aust. J. Earth Sci. 54, 541–559. https://doi.org/10.1080/08120090601078388

Fraser, R., Wells, R., 2006. Palaeontological excavation and taphonomic investigation of the late Pleistocene fossil deposit in Grant Hall, Victoria Fossil Cave, Naracoorte, South Australia. Alcheringa An Australas. J. Palaeontol. 30, 147–161. https://doi.org/10.1080/03115510609506860

Galbraith, R. F., Roberts, R. G., Laslett, G. M., Yoshida, H., & Olley, J.M., 1999. Optical Dating Of Single And Multiple Grains Of Quartz From Jinmium Rock Shelter, Northern Australia: Part I, Experimental Design And Statistical Models*. Archaeometry 41, 339–364. https://doi.org/10.1111/j.1475-4754.1999.tb00987.x

Grün, R., Moriarty, K., Wells, R., 2001. Electron spin resonance dating of the fossil deposits in the Naracoorte Caves, South Australia. J. Quat. Sci. 16, 49–59.

Guérin, G., Mercier, N., Adamiec, G., 2011. Dose-rate conversion factors: Update. Anc. TL 29, 5–8.

Guilarte, V., Fang, F., Grün, R., Duval, M., 2021. ESR dating of quartz grains: evaluating the performance of various cryogenic systems for dosimetric purpose. Submitted

Jacobs, Z., Duller, G.A.T., Wintle, A.G., Henshilwood, C.S., 2006. Extending the chronology of deposits at Blombos Cave, South Africa, back to 140ka using optical dating of single and multiple grains of quartz. J. Hum. Evol. 51, 255–273. https://doi.org/https://doi.org/10.1016/j.jhevol.2006.03.007

Lisiecki, L.E., Raymo, M.E., 2005. A Pliocene-Pleistocene stack of 57 globally distributed benthic δ18O records. Paleoceanography 20, n/a-n/a. https://doi.org/10.1029/2004PA001071

Macken, A.C., Jankowski, N.R., Price, G.J., Bestland, E.A., Reed, E.H., Prideaux, G.J., Roberts, R.G., 2011. Application of sedimentary and chronological analyses to refine the depositional context of a Late Pleistocene vertebrate deposit, Naracoorte, South Australia. Quat. Sci. Rev. 30, 2690–2702. https://doi.org/https://doi.org/10.1016/j.quascirev.2011.05.023

McCluskey, C., 2012. Cave sediments as Palaeoenvironmental Indicators: Alexandra Cave, Naracoorte, South Australia.

Mejdahl, V., 1979. Thermoluminescence Dating: Beta-Dose Attenuation In Quartz Grains. Archaeometry 21, 61–72. https://doi.org/https://doi.org/10.1111/j.1475-4754.1979.tb00241.x

Moriarty, K.C., McCulloch, M.T., Wells, R.T., McDowell, M.C., 2000. Mid-Pleistocene cave fills, megafaunal remains and climate change at Naracoorte, South Australia: towards a predictive model using U-Th dating of speleothems. Palaeogeogr. Palaeoclimatol. Palaeoecol. 159, 113–143. https://doi.org/https://doi.org/10.1016/S0031-0182(00)00036-5

Prescott, J.R., Hutton, J.T., 1994. Cosmic ray contributions to dose rates for luminescence and ESR dating: Large depths and long-term time variations. Radiat. Meas. 23, 497–500. https://doi.org/10.1016/1350-4487(94)90086-8

Prideaux, G.J., Roberts, R., Megirian, D., Westaway, K., Hellstrom, J., Olley, J., 2007. Mammalian responses to Pleistocene climate change in southeastern Australia. Geology 35, 33–36. https://doi.org/10.1130/G23070A.1

Reed, E., Bourne, S., 2009. Pleistocene fossil vertebrate sites of the south-east region of South Australia II. Trans. R. Soc. South Aust. 133, 30–40.

Reed, E., Bourne, S., 2000. Pleistocene fossil vertebrate sites of the South-East region of South Australia. Trans. R. Soc. South Aust. 124, 61–90.

Richter, M., Tsukamoto, S., 2021. Investigation of quartz ESR residual signals in the last glacial and early Holocene fluvial deposits from the Lower Rhine. Geochronol. Discuss. 2021, 1–15. https://doi.org/10.5194/gchron-2021-9

Rink, W.J., Bartoll, J., Schwarcz, H.P., Shane, P., Bar-Yosef, O., 2007. Testing the reliability of ESR dating of optically exposed buried quartz sediments. Radiat. Meas. 42, 1618–1626.

Rittner, S., 2013. The efficacy of electron spin resonance for the dating of quartz. A case study of aeolianites of the bridgewater formation in southeastern south australia. University of New South Wales.

Russell, N.J., Armitage, S.J., 2012. A comparison of single-grain and small aliquot dating of fine sand from Cyrenaica, northern Libya. Quat. Geochronol. 10, 62–67.

Saltré, F., Rodríguez-Rey, M., Brook, B.W., Johnson, C.N., Turney, C.S.M., Alroy, J., Cooper, A., Beeton, N., Bird, M.I., Fordham, D.A., Gillespie, R., Herrando-Pérez, S., Jacobs, Z., Miller, G.H., Nogués-Bravo, D., Prideaux, G.J., Roberts, R.G., Bradshaw, C.J.A., 2016. Climate change not to blame for late Quaternary megafauna extinctions in Australia. Nat. Commun. 7. https://doi.org/10.1038/ncomms10511

St Pierre, E., Zhao, J.X., Feng, Y.X., Reed, E., 2012. U-series dating of soda straw stalactites from excavated deposits: Method development and application to Blanche Cave, Naracoorte, South Australia. J. Archaeol. Sci. 39, 922–930. https://doi.org/10.1016/j.jas.2011.10.027

Stone, A.E.C., Bailey, R.M., 2012. The effect of single grain luminescence characteristics on single aliquot equivalent dose estimates. Quat. Geochronol. 11, 68–78.

Tanaka, K., Hataya, R., Spooner, N.A., Questiaux, D.G., Saito, Y., Hashimoto, T., 1997. Dating of marine terrace sediments by ESR, TL and OSL methods and their applicabilities. Quat. Sci. Rev. 16, 257–264. https://doi.org/https://doi.org/10.1016/S0277-3791(96)00092-3

Tanaka, K., Machette, M.N., Crone, A.J., Roger Bowman, J., 1995. ESR dating of aeolian sand near tennant creek, Northern territory, Australia. Quat. Sci. Rev. 14, 385–393.

Tissoux, H., Falguères, C., Voinchet, P., Toyoda, S., Bahain, J.J., Despriée, J., 2007. Potential use of Ti-center in ESR dating of fluvial sediment. Quat. Geochronol. 2, 367–372. https://doi.org/10.1016/j.quageo.2006.04.006

Tissoux, H., Toyoda, S., Falguères, C., Voinchet, P., Takada, M., Bahain, J.-J., Despriée, J., 2008. ESR Dating of Sedimentary Quartz from Two Pleistocene Deposits Using Al and Ti-Centers. Geochronometria 30, 23–31.

Tissoux, H., Valladas, H., Voinchet, P., Reyss, J.L., Mercier, N., Falguères, C., Bahain, J.-J., Zöller, L., Antoine, P., 2010. OSL and ESR studies of Aeolian quartz from the Upper Pleistocene loess sequence of Nussloch (Germany). Quat. Geochronol. 5, 131,136.

Toyoda, S., Voinchet, P., Falguères, C., Dolo, J.M., Laurent, M., 2000. Bleaching of ESR signals by the sunlight: a laboratory experiment for establishing the ESR dating of sediments. Appl. Radiat. Isot. 52, 1357–1362. https://doi.org/10.1016/S0969-8043(00)00095-6

Tsukamoto, S., Porat, N., Ankjærgaard, C., 2017. Dose recovery and residual dose of quartz ESR signals using modern sediments: Implications for single aliquot ESR dating. Radiat. Meas. 106, 472–476. https://doi.org/https://doi.org/10.1016/j.radmeas.2017.02.010

White, S., Webb, J.A., 2015. The influence of tectonics on flank margin cave formation on a passive continental margin: Naracoorte, Southeastern Australia. Geomorphology 229, 58–72.

Yoshida, H., 1996. Quaternary dating studies using ESR signals, with emphasis on shell, coral, tooth enamel and quartz. Australian National University, Canberra, Australia.

Figures

Figure 1. Stratigraphy of entire sedimentary infill deposit from entrance chamber of Alexandra Cave, Naracoorte Caves, South Australia, including photos, sample position (A1, A2, A3) and locality of fossilised fauna (indicated by bone symbols). B: Specimen Cave photo and sample position C: Whale Bone Cave sample position and photos. Yellow circles indicate combined OSL–ESR sample positions, and are approximately 4 cm in diameter. Geographical location of cave sites are shown in Figure S1.

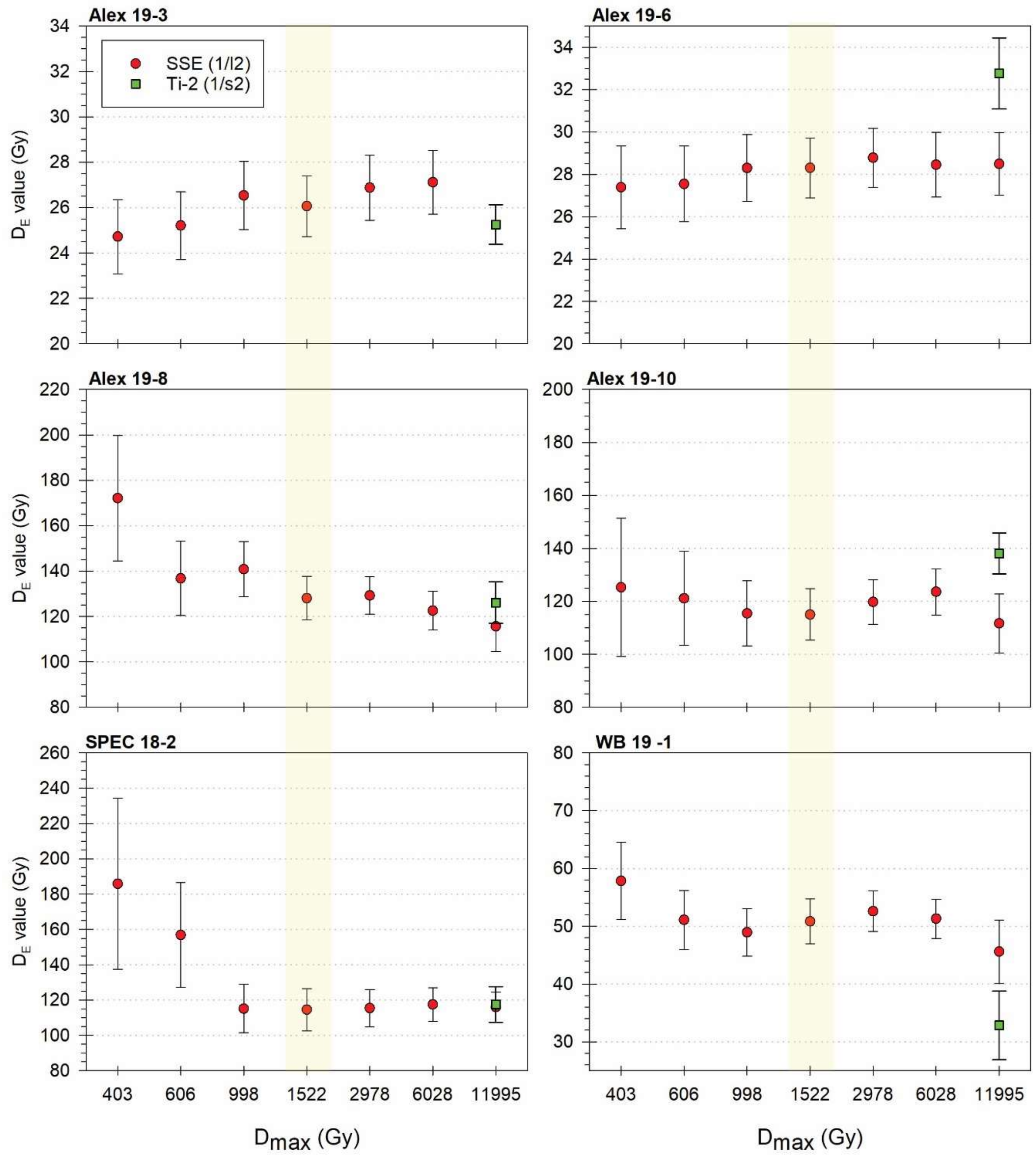

Figure 2. D_e values obtained for the Ti-H signal and derived from SSE (red circles) and Ti-2 (green squares) fitting functions, with maximum irradiation dose (D_{max}) varying between 400 and 12000 Gy. D_e value is considered reliable in the D_{max} range for which D_e values remain constant. All samples show constant D_e values between D_{max} of 600-6000 Gy. D_e values used for age calculations are derived from the SSE ($1/I^2$) with D_{max} = 1500 Gy (highlighted in yellow).

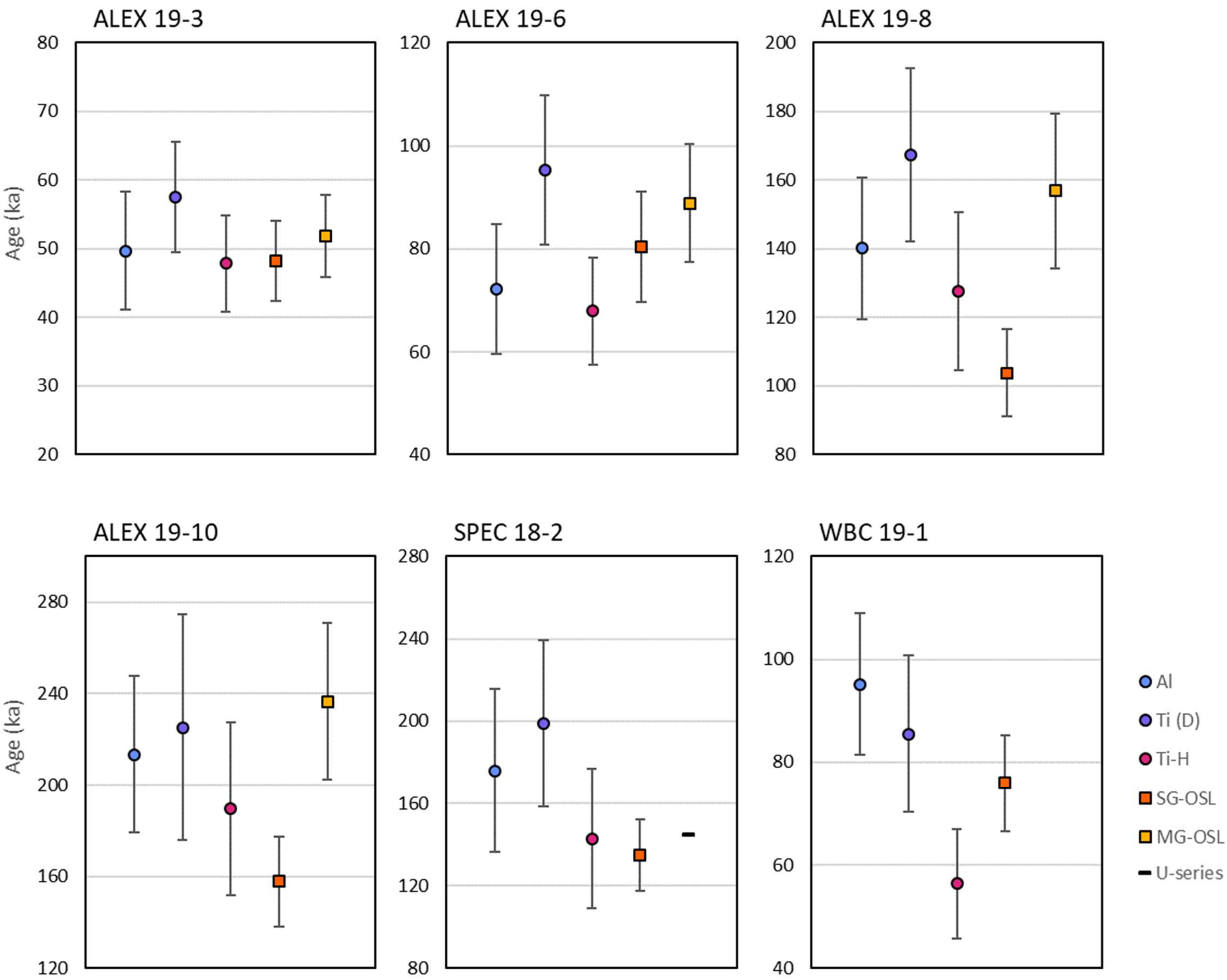

Figure 3. Comparison of final MG OSL, SG OSL and MC ESR ages for each sample, represented as mean ± total uncertainty at 95% confidence interval. The U-series ages (SP 17 = 145 ± 3.5 ka, and SP 18 = 142.8 ± 2.1 ka) for SPEC 18-2 has been derived from the capping flowstone immediate overlying the OSL-ESR sample, and therefore represents a close minimum age constraint (Table S5).

Table

Table 1. Summary statistics of radionuclide concentrations, environmental dose rates, D_e measurements and final OSL and ESR samples. OSL and ESR uncertainties are quoted at 1σ. Field water content is expressed as percentage of dry mass mineral fraction with ± 20% uncertainty. Gamma dose rates were calculated from in situ measurements made at each sampling position using a NaI:Tl detector. Beta dose rates were calculated using a Risø GM-25-5 low-level beta counter. Individual radionuclide concentrations were derived from the field gamma spectra using the 'energy windows' method (Arnold et al., 2012a). Cosmic dose rates were calculated by taking into account the geomagnetic latitude, altitude and thickness of overburden (Prescott & Hutton, 1994). The gamma, beta and cosmic-ray dose rates are corrected for long-term sediment water content (Aitken, 1985). The total dose rate for the luminescence samples includes an empirically determined internal dose rate of 0.04 Gy/ka (Arnold et al., this volume) with an uncertainty of 30% (Bowler et al., 2003). SG OSL and MG OSL D_e datasets and overdispersion values are calculated using the central age model (CAM) (Galbraith et al., 1999). The total dose rate for ESR samples include an empirically determined internal dose of 0.06 +/- 0.01 Gy/ka (Arnold et al., this volume) using an alpha efficiency of 0.07 ± 0.01 (1σ) for both the Al and Ti centres (Bartz et al., 2019). U-series ages are presented here with 2σ uncertainty, see Table S5 for details.

Sample	Alex 19-3	Alex 19-6	Alex 19-8	Alex 19-10	SPEC 18-2	WBC 19-1
Unit	C	E	F	G	-	-
Depth (cm)	262	411	473	585	85	20
Water content (%)	3.6 ± 0.7	3.3 ± 0.7	11.1 ± 2.2	6.0 ± 1.2	16.5 ± 3.3	16.2 ± 3.2
Internal dose rate (ESR) (Gy/ka)	0.06 ± 0.02	0.06 ± 0.02	0.06 ± 0.02	0.06 ± 0.02	0.06 ± 0.02	0.06 ± 0.02
Internal dose rate (OSL) (Gy/ka)	0.04 ± 0.01	0.04 ± 0.01	0.04 ± 0.01	0.04 ± 0.01	0.04 ± 0.01	0.04 ± 0.01
Beta dose rate (ESR) (Gy/ka)	0.24 ± 0.01	0.15 ± 0.01	0.53 ± 0.03	0.27 ± 0.02	0.29 ± 0.02	0.41 ± 0.02
Grain size (µm)	125 – 212	125 – 212	125 – 212	125 – 212	212 – 250	90 – 250
Beta dose rate (OSL) (Gy/ka)	0.23 ± 0.01	0.15 ± 0.01	0.51 ± 0.03	0.26 ± 0.03	0.29 ± 0.02	0.41 ± 0.02
Grain size (µm)	212 – 250	212 – 250	212 – 250	212 – 250	212 – 250	90 – 250
Gamma dose rate (Gy/ka)	0.20 ± 0.01	0.16 ± 0.01	0.37 ± 0.02	0.24 ± 0.01	0.40 ± 0.02	0.38 ± 0.02
Cosmic dose rate (Gy/ka)	0.05 ± 0.01	0.05 ± 0.01	0.04 ± 0.00	0.04 ± 0.00	0.06 ± 0.01	0.06 ± 0.02
Total dose rate (ESR) (Gy/ka)	0.54 ± 0.03	0.42 ± 0.02	1.00 ± 0.05	0.61 ± 0.03	0.80 ± 0.05	0.90 ± 0.05
Total dose rate (OSL) (Gy/ka)	0.51 ± 0.03	0.39 ± 0.02	0.96 ± 0.05	0.58 ± 0.03	0.78 ± 0.04	0.88 ± 0.05
D_e (Gy) Al	27.0 ± 1.9	30.1 ± 2.0	140.7 ± 7.4	129.4 ± 7.9	141.0 ± 13.4	85.8 ± 4.0
D_e (Gy) Ti (D)	31.3 ± 1.4	39.7 ± 1.9	168.2 ± 9.3	136.6 ± 13.1	159.4 ± 13.1	77.0 ± 5.3
D_e (Gy) Ti-H	26.1 ± 1.3	28.3 ± 1.4	128.1 ± 9.5	115.0 ± 9.7	114.5 ± 12.0	50.8 ± 3.9
D_e (Gy) SG OSL	24.8 ± 0.6	31.3 ± 1.0	99.8 ± 2.9	90.7 ± 2.5	105.0 ± 2.6	66.7 ± 1.4
Overdispersion (%)	26.4 ± 2.1	40.6 ± 2.4	26.8 ± 2.5	26.4 ± 2.3	30.0 ± 1.9	25.9 ± 1.6
D_e (Gy) MG OSL	26.7 ± 0.6	34.7 ± 0.8	150.9 ± 7.0	136.0 ± 6.3	-	-
Overdispersion (%)	0	0	6.6 ± 5.6	0	-	-
Age (ka) Al	49.7 ± 4.3	72.3 ± 6.3	140.2 ± 10.3	213.4 ± 17.1	175.8 ± 19.4	95.2 ± 6.9
Age (ka) Ti (D)	57.5 ± 4.0	95.3 ± 7.2	167.5 ± 12.6	225.3 ± 24.7	198.8 ± 19.8	85.5 ± 7.6

Age (ka) Ti-H	47.9 ± 3.5	67.9 ± 5.2	127.6 ± 11.5	189.6 ± 18.9	142.8 ± 17.0	56.4 ± 5.3
Age (ka) MG OSL	51.9 ± 3.0	88.9 ± 5.7	156.9 ± 11.3	236.5 ± 17.1	-	-
Age (ka) SG OSL	48.2 ± 2.9	80.4 ± 5.4	103.8 ± 6.4	157.8 ± 9.8	134.7 ± 8.7	75.9 ± 4.7
Age (ka) U-series					145.0 ± 3.5	
					142.8 ± 2.1	